as the surface oxidation reaction

$$nCeO_x\ (x < 2,\ n > 1) + O_2 \rightarrow [nCeO_x]^+O_2^- \rightarrow [nCeO_x]^{2+}O_2^{2-} \rightarrow [nCeO_x]^{2+} + 2O^- \rightarrow nCeO_y\ (x < y \leq 2)$$

Apparently, over the more oxygen-deficient CeO_x, i.e., the smaller x, the reactions proceed more potentially to form O_2^- and O_2^{2-} species. It is quite possible that the peroxide is formed in two ways on the partially reduced cerium oxide. One is via the interaction between two O_2^-, and the other is through the further accepting of an electron of O_2^- by virtue of oxidation of the surface site as described in the above sequence. It is generally considered that O_2^- is bent bonded and O_2^{2-} is side-on bonded on metal surfaces.[41] The abundance of O_2^{2-} on partially reduced cerium oxide may be accounted for by an adsorption model; that is, the peroxide species are formed via the interaction of O_2 with two neighboring Ce^{3+} sites. This can also be explained as follows: the peroxide species are generated via the O_2^- formed on Ce^{3+} or a defect site and subsequently interact with a defect or a Ce^{3+} site in the vicinity where the O_2^{2-} gains its second electron. Since the defect sites on CeO_2 (1000 K) are more sparse than those on CeO_2 (673-H), the peroxide are unfavorable on the former. It is reasonable that the amount of adsorbed peroxide increases with reduction time of cerium oxide (Figure 5) because more surface defects and oxygen vacancy are produced after deeper prereduction. Obviously the CeO_2 (673-H) is more ready to contribute electron to oxygen than is CeO_2 (1000 K); therefore, the O_2^{2-} species are favored on the former. These results are in accordance with the conclusions[42] from molecular orbital calculations for metal complexes in which the peroxide ligand only forms on central metal with low oxidation state. Figure 5 shows that the amount of adsorbed O_2^- remains almost unchanged on various cerium oxide with different degrees of reduction, and this could be interpreted in terms of the conversion from O_2^- to O_2^{2-} that limits the surface concentration of O_2^-.

A similar tendency to the results shown in Figure 2 was found for the band at 883 cm^{-1} in Figure 5, which indicates the conversion from O_2^{2-} to O^- and $O^{2-}{}_{lc}$ and the surface is successively oxidized. The two reverse bands at 2115 and 939 cm^{-1} (Figure 4) appear after admission of O_2 to partially reduced cerium oxide and become more intense with higher adsorption temperature. This fact indicates that the surface is reoxidized at elevated temperatures.

Conclusions

The adsorption of oxygen on well-outgassed cerium oxide gives rise to the IR bands at 2237 and 1126 cm^{-1} attributed to superoxide species and on partially reduced cerium oxide produces the IR bands at 2239, 1128, and 883 cm^{-1} attributed to superoxide and peroxide species, respectively. The assignments are confirmed by the spectra of isotopic $^{18}O_2$ adsorption. The nature of adsorption sites suggests that the superoxide species are formed on the surface defects, namely, the coordinately unsaturated Ce^{4+} ions, and the peroxide species on Ce^{3+} ions or on Ce^{3+} and Ce^{4+} with oxygen nest. The conversion from O_2^- to O_2^{2-} is proposed in two ways: a disproportionation reaction of O_2^- and a successively accepting electron from the surface. The former is universal on both the surfaces of CeO_2 (1000 K) and CeO_2 (673-H); however, the latter particularly happens on the reduced surface.

Acknowledgment. C.L. is indebted to the Ministry of Education, Science and Culture of Japan and the United Nations Educational, Scientific and Cultural Organization (UNESCO) for the work finished when he was a research fellow during its 23rd International Postgraduate University Course in Chemistry and Chemical Engineering held at Tokyo Institute of Technology, Tokyo, Japan, during 1987–1988.

(41) Albert, M. R.; Yates, J. T., Jr. *The Surface Scientist's Guide to Organometallic Chemistry*; American Chemical Society: Washington, DC, 1987; p 40.
(42) Boca, R. *Coord. Chem. Rev* **1983**, *50*, 1.

Optical Spectra of Transition-Metal Carbonyls: $Cr(CO)_6$, $Fe(CO)_5$, and $Ni(CO)_4$

Manfred Kotzian,[†] Notker Rösch,*[,†] Hartmut Schröder,*[,‡] and Michael C. Zerner[§]

Contribution from the Lehrstuhl für Theoretische Chemie, Technische Universität München, D-8046 Garching, Federal Republic of Germany, Max-Planck-Institut für Quantenoptik, D-8046 Garching, Federal Republic of Germany, and Quantum Theory Project, University of Florida, Gainesville, Florida 32611. *Received March 7, 1989*

Abstract: Near-UV gas-phase optical spectra and absolute absorption cross sections of the transition-metal carbonyls $Cr(CO)_6$, $Fe(CO)_5$, and $Ni(CO)_4$ are presented. They have been recorded using a fast-scanning spectral photometer to minimize heterogeneous decomposition during the measurement. The excited states in the experimental energy range were analyzed employing an INDO/S CI formalism. Calculations on the basis of single excitation CI for singlet–singlet transitions yield good agreement both for transition energies and intensities. From these theoretical models it is deduced that transition-metal carbonyl near-UV spectra are determined exclusively by metal-to-ligand charge-transfer transitions, whereas d → p and d → s excitations do not contribute significantly below 6.2 eV (above 200 nm). The lowest lying singlet excitations in $Cr(CO)_6$ and $Fe(CO)_5$ are predicted to be d → d. Although they are predicted to have little or no dipole allowed character, they should be observable because they are well separated from the first allowed bands. Indeed, they have been detected for $Cr(CO)_6$. The spectra of several substituted complexes $(CO)_5CrR$ (R = CS, PF_3, CHOH) are also calculated and compared with available experimental data.

In the last few years transition-metal carbonyls gained increasing importance in laser chemistry as a source of metal atoms or reactive precursors for chemical vapor deposition of thin films or layers on surfaces.[1] For the analysis of reaction mechanisms it is necessary to understand the electronic structure both of the carbonyls and their fragment molecules. Extended Hückel-type[2] and CNDO CI[3] calculations have been used as basis for the interpretation of experimental UV absorption spectra[4–7] of various

[†] Technische Universität München.
[‡] Max-Planck-Institut für Quantenoptik.
[§] University of Florida.

(1) (a) Kompa, K. L. *Angew. Chem.* **1988**, *100*, 1287. (b) Schröder, H.; Rager, B.; Metev, S.; Rösch, N.; Jörg, H. In *Interfaces Under Laser Irradiation*; Laude, L. D., Bäuerle D., Wautelet, M., Eds.; Martinus Nijhoff Publishers: Dordrecht, The Netherlands, 1987; p 255.
(2) Schreiner, A. F.; Brown, T. C. *J. Am. Chem. Soc.*, **1968**, *90*, 3366.
(3) Dick, B.; Freund, H.-J.; Hohlneicher, G. *Mol. Phys.* **1982**, *45*, 427.
(4) Beach, N. A.; Gray, H. B. *J. Am. Chem. Soc.* **1968**, *90*, 5713.

0002-7863/89/1511-7687$01.50/0

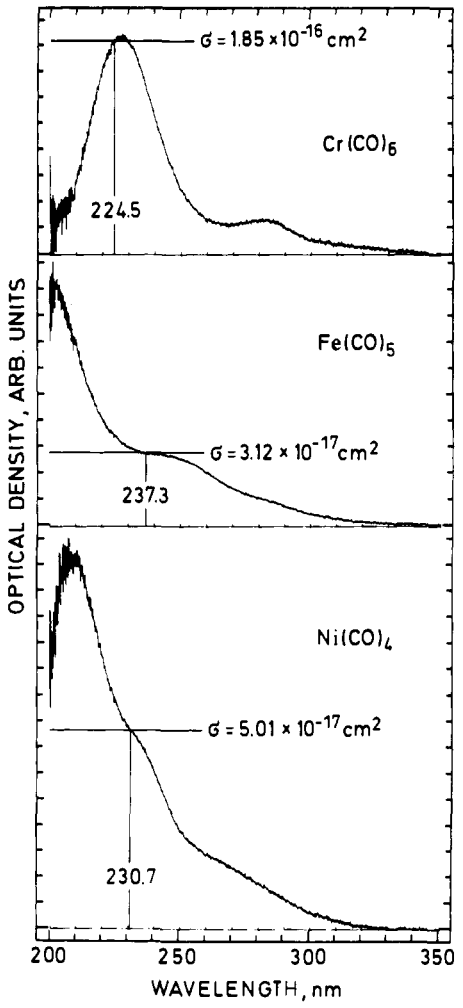

Figure 1. Absorption spectra of $Cr(CO)_6$, $Fe(CO)_5$, and $Ni(CO)_4$. The relative error of the absorption cross sections is less than 1%.

transition-metal carbonyls—neutral, charged, or radicals. Also experimentally and calculationally based photofragmentation mechanisms of electronically excited carbonyl molecules have been proposed.[8-17] In this paper we will concentrate on the near-UV spectra of the key transition-metal carbonyl compounds $Cr(CO)_6$, $Fe(CO)_5$, and $Ni(CO)_4$ and on the interpretation of their spectra (shown in Figure 1) since a thorough knowledge of the excited state is of pivotal importance for the understanding of further fragmentation processes. Previous interpretations of these UV spectra have often been tentative, being restricted to general characterizations of spectral bands as charge-transfer excitations. Detailed assignments are rarely given.[4]

As our theoretical tool we will employ the intermediate neglect of differential overlap model adopted for spectroscopy[18] (INDO/S)

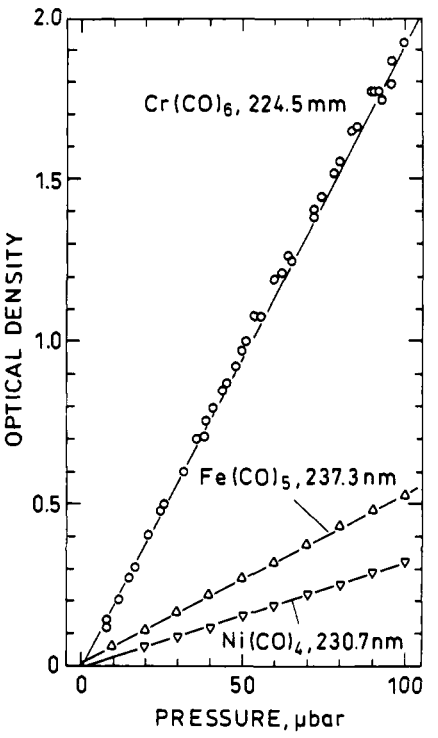

Figure 2. Increase of optical density with pressure for: $Cr(CO)_6$, 304 K; $Fe(CO)_5$, 301 K; $Ni(CO)_4$, 302 K. Cell length 10.0 cm. The solid lines are fitted to the data points.

that has been shown to be useful and reliable for studying the excited states of organic molecules,[18,19] transition-metal compounds,[20-24] and larger complexes, such as transition-metal porphyrins.[25-27] In the following, results will be presented from applications to a class of complexes with σ-donator π-acceptor ligands, where the correct description of charge donation and back-donation is essential, adding further credit to the INDO/S method.

Experimental Details

It is well-known that carbonyls tend to heterogeneously decompose in static cells, in particular at low pressure, according to $M(CO)_x \rightarrow M + xCO$. Therefore, it is often difficult to determine the correct partial pressure of the carbonyls from the total pressure and, hence, to accurately determine the absorption cross section. Our cell was directly connected to a vacuum line and a filling station. It was 10.0 cm long and equipped with quartz windows. The applied pressure was measured with a calibrated Baratron capacitance manometer. The spectra were recorded with a computer-aided scanning spectral photometer from Bruins Instruments. The scan speed for a single sweep was about 0.2 s.

After the recording of a carbonyl spectrum the sample gas was rapidly cooled with a liquid-nitrogen trap. The persistent pressure is then essentially due to carbon monoxide from the composition of carbonyl molecules during one experimental cycle, equivalent to a period of about 3 min. It was typically 1.5% for $Cr(CO)_6$, 2% for $Fe(CO)_5$, and 10% for $Ni(CO)_4$. The difference between this pressure and the primarily applied carbonyl pressure was taken as the true carbonyl pressure of the recorded spectrum.

The increase of optical densities of $Cr(CO)_6$ at 224.5 nm, $Fe(CO)_5$ at 237.3 nm, and $Ni(CO)_4$ at 230.7 nm for increasing difference pressures

(5) Dartiguenave, M.; Dartiguenave, Y.; Gray, H. B. *Bull. Soc. Chim. Fr.* **1969**, 4223.
(6) Gray, H. B. Beach, N. A. *J. Am. Chem. Soc.* **1963**, *85*, 2922.
(7) Lever, A. B. P. *Inorganic Electronic Spectroscopy*, 2nd ed.; Elsevier: New York, 1986.
(8) Rösch, N.; Kotzian, M.; Jörg, H.; Schröder, H.; Rager B.; Metev, S. *J. Am. Chem. Soc.* **1986**, *108*, 4238.
(9) Elian, M.; Hoffmann, R. *Inorg. Chem.* **1975**, *14*, 1058.
(10) Thompson, H. W.; Garret, A. A. *J. Chem. Soc.* **1934**, 1817; 1822.
(11) Callear, A. B. *Proc. R. Soc. A* **1961**, *265*, 71.
(12) Čarsky, P.; Dedieu, A. *Chem. Phys.* **1986**, *103*, 265.
(13) (a) Seder, T. A.; Church, S. P.; Weitz, E. *J. Am. Chem. Soc.* **1986**, *108*, 4721. (b) Seder, T. A.; Ouderkirk, A. J.; Weitz, E. *J. Chem. Phys.* **1986**, *85*, 1977.
(14) (a) Antolovic, D.; Davidson, E. R. *J. Chem. Phys.* **1988**, *88*, 4967. (b) Antolovic, D.; Davidson, E. R. *J. Am. Chem. Soc.* **1987**, *109*, 977.
(15) (a) Lees, A. J. *J. Am. Chem. Soc.* **1982**, *104*, 2038. (b) Lees, A. J.; Adamson, A. W. *J. Am. Chem. Soc.* **1982**, *104*, 3804.
(16) Waller, I. M.; Hepburn, J. W. *J. Chem. Phys.* **1988**, *88*, 6058.
(17) Tyndall, G. W.; Jackson, R. L. *J. Chem. Phys.* **1988**, *89*, 1364.
(18) Ridley, J.; Zerner, M. C. *Theor. Chim. Acta* **1976**, *42*, 223.
(19) Ridley, J.; Zerner, M. C. *Theor. Chim. Acta* **1973**, *32*, 111.
(20) Bacon, A. D.; Zerner, M. C. *Theor. Chim. Acta* **1979**, *53*, 21.
(21) Anderson, W. P.; Edwards, W. D.; Zerner, M. C. *Inorg. Chem.* **1986**, *25*, 2728.
(22) Zerner, M. C.; Loew, G. H.; Kirchner, R. F.; Mueller-Westerhoff, U. T. *J. Am. Chem. Soc.* **1980**, *102*, 589.
(23) Edwards, W. D.; Zerner, M. C. *Int. J. Quantum Chem.* **1983**, *23*, 1407.
(24) Edwards, W. D.; Zerner, M. C. *Can. J. Chem.* **1985**, *63*, 1763.
(25) Loew, G. H.; Herman, Z. S.; Zerner, M. C. *Int. J. Quantum Chem.* **1980**, *17*, 481.
(26) Edwards, W. D.; Weiner, B.; Zerner, M. C. *J. Am. Chem. Soc.* **1986**, *108*, 2196.
(27) Waleh, A.; Collins, J. R.; Loew, G. H.; Zerner, M. C. *Int. J. Quantum Chem.* **1986**, *29*, 1575.

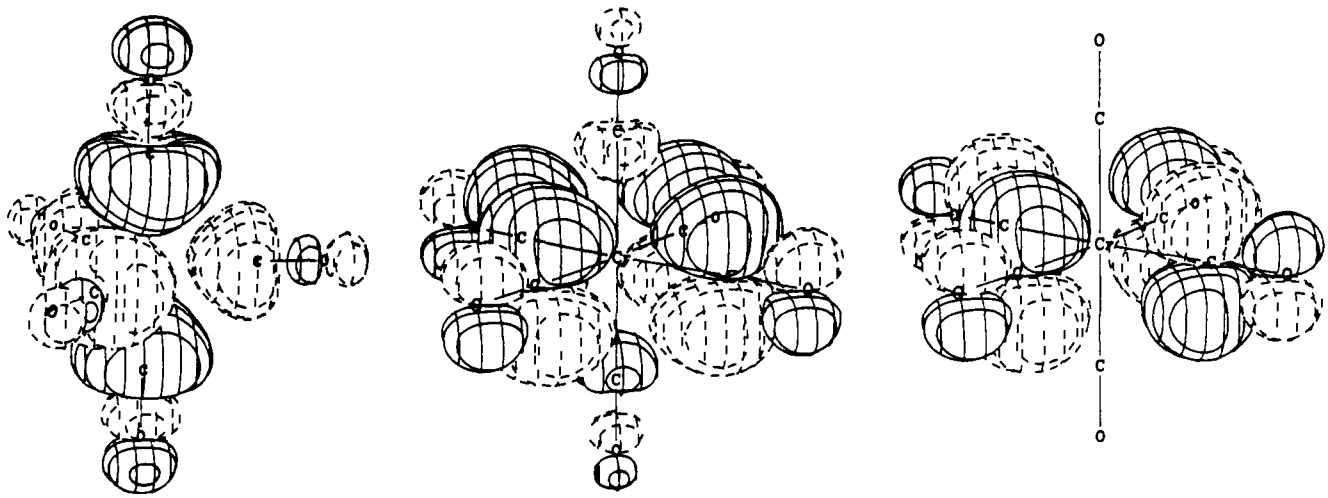

Figure 3. (a) Contour plot of the $13a_1'$ orbital of iron pentacarbonyl. (b) Contour plot of the z component of the $9t_{1u}$ orbital of chromium hexacarbonyl. (c) Contour plot of the z component of the $2t_{2u}$ orbital of chromium hexacarbonyl.

is shown in Figure 2. The solid lines are calculated from a linear regression routine. From the slopes of these lines, the measured cell temperatures, and the ideal gas law the corresponding absorption cross section could be evaluated with high accuracy. Those data are utilized as scale factors of the carbonyl spectra, which are shown in Figure 1.

The relative accuracy is better than 1%, whereas the absolute cross sections depend on the absolute calibration and stability of our manometer. We have compared different systems for different gases and vapors. On the basis of this experience, we estimate the absolute error to be less than 10%. The increasing noise of the blue end of the spectra in Figure 1 is due to the decreasing spectral intensity of the deuterium lamp.

Computational Method

The details of the INDO/S method, including the parametrization and the technique for calculating electronic spectra, are given elsewhere.[18-22] For the benefit of the reader the salient features of INDO/S will be briefly summarized here for the closed-shell case. The Fock operator (eq 1)

$$F_{\mu\mu} = U_{\mu\mu} + \sum_{\sigma,\lambda}^{A} P_{\sigma\lambda}[(\mu\mu|\sigma\lambda) - \tfrac{1}{2}(\mu\sigma|\mu\lambda)] + \sum_{B\neq A} (P_{BB} - Z_B)\gamma_{AB} \qquad \mu\in A$$

$$F_{\mu\nu} = \sum_{\sigma,\lambda}^{A} P_{\sigma\lambda}[(\mu\nu|\sigma\lambda) - \tfrac{1}{2}(\mu\sigma|\nu\lambda)] \qquad \mu, \nu\in A$$

$$F_{\mu\nu} = \tfrac{1}{2}(\beta_A + \beta_B)\bar{S}_{\mu\nu} - \tfrac{1}{2}P_{\mu\nu}\gamma_{AB} \qquad \mu\in A, \nu\in B \qquad (1)$$

in the INDO approximation is used to calculate the ground state in terms of molecular orbital coefficients and eigenvalues with

$$(\mu\nu|\sigma\lambda) = \int d\tau_1 \int d\tau_2\, \chi_\mu^*(1)\, \chi_\nu(1)\, r_{12}^{-1}\, \chi_\sigma(2)\, \chi_\lambda(2)$$

The one-center core integrals $U_{\mu\mu}$ are taken from experimental atomic ionization potentials[28,29] and thus incorporate the effects of the one-center core effective potential $V_{\mu\mu}$.[30] In the case of transition metals with s, p, and d orbitals, there are two possible processes of ionization depending on the configuration of the metal atom ($d^{n-2}s^2$, $d^{n-1}s^1$). A procedure has been developed[22] to include both processes in the semiempirical determination of the one-center core integrals. The relative contribution of each process is determined by the relative energies of the two ground-state configurations. The two-center two-electron integrals are taken from the Weiss–Mataga–Nishimoto formula[31]

$$\gamma_{AB} = \frac{1.2}{2.4/(\gamma_{AA} + \gamma_{BB}) + R_{AB}} \qquad (2)$$

in which the Pariser approximation[32] is adopted for the one-center two-electron integrals

$$\gamma_{AA} = F^0(AA) = I_A - A_A \qquad (3)$$

The resulting parameters for the first-row transition-metal series are given in ref 21. It has been found useful[20] to refine the parametrization of the resonance integrals as follows. Each transition-metal atom A is assigned two resonance parameters, $\beta_s(A) = \beta_p(A) \neq \beta_d(A)$, and these values are adjusted to reproduce the experimental molecular spectra. $\bar{S}_{\mu\nu}$ is related to the overlap matrix element $S_{\mu\nu}$

$$\bar{S}_{\mu\nu} = \sum f_{lm} g_{lm} S_{\mu(m)\nu(m)} \qquad (4)$$

in which g_{lm} is a Eulerian transformation matrix element required to rotate the orbitals from the local coordinate system to the molecular system, f_{lm} is an empirical factor improving the ordering of σ and π type orbitals,[18,19] and $S_{\mu(m)\nu(m)}$ is the σ, π, or δ component of the overlap integrals in the local system. The values adopted for f_{lm} are[18] $f_{p\sigma} = 1.267$ and $f_{p\pi} = 0.640$. All one-center two-electron integrals (Slater–Condon factors) on any given metal center are included in the calculation.[33]

Ionization potentials are estimated using Koopmans' theorem. The electronic spectra are calculated from the self-consistent-field (SCF) ground state by invoking a virtual orbital configuration interaction (CI) procedure resulting in the desired spectroscopic transition energies and oscillator strengths. The latter quantities are evaluated using the one-center dipole length integrals. All single excitations of the valence orbitals are included in the CI calculation (full CIS). For the reproduction of the spectra only singlet–singlet transitions are considered. Therefore, the multiplicity is not indicated in the case of singlet states, for brevity. Only single–triplet transitions up to the first singlet excitation are discussed to complement the theoretical spectrum.

Rydberg-type states cannot be described properly by the present INDO/S procedure, since Rydberg-type orbitals are not included in the atomic basis. For the carbonyl compounds Rydberg states might be expected to appear about 2 eV below the first ionization potential.[22] Therefore, they are unlikely observed in our spectral range. Since Rydberg states carry little or no intensity of their own, they will not affect the main features of the calculated spectra. They may be expected to borrow intensity through configurational mixing with more intense singly excited valence states. For a more detailed discussion concerning the influence of Rydberg states on calculated spectra, see ref 22.

Higher excitations are neglected since their influence is taken into account through the choice of semiempirical two-electron integrals γ and empirical resonance integrals β.[22] But no such

(28) Moore, C. E. *Atomic Energy Levels*; National Bureau of Standards: Washington, DC, 1949.
(29) Karlson, G.; Zerner, M. C. *Int. J. Quantum Chem.* **1973**, *7*, 35.
(30) Zerner, M. C. *Mol. Phys.* **1972**, *23*, 963.
(31) Mataga, N.; Nishimoto, K. *Z. Phys. Chem.* **1957**, *13*, 140.
(32) Pariser, R.; Parr, R. *J. Chem. Phys.* **1953**, *21*, 767.
(33) Culberson, J. C.; Knappe, P.; Rösch, N.; Zerner, M. C. *Theor. Chim. Acta* **1987**, *71*, 21.

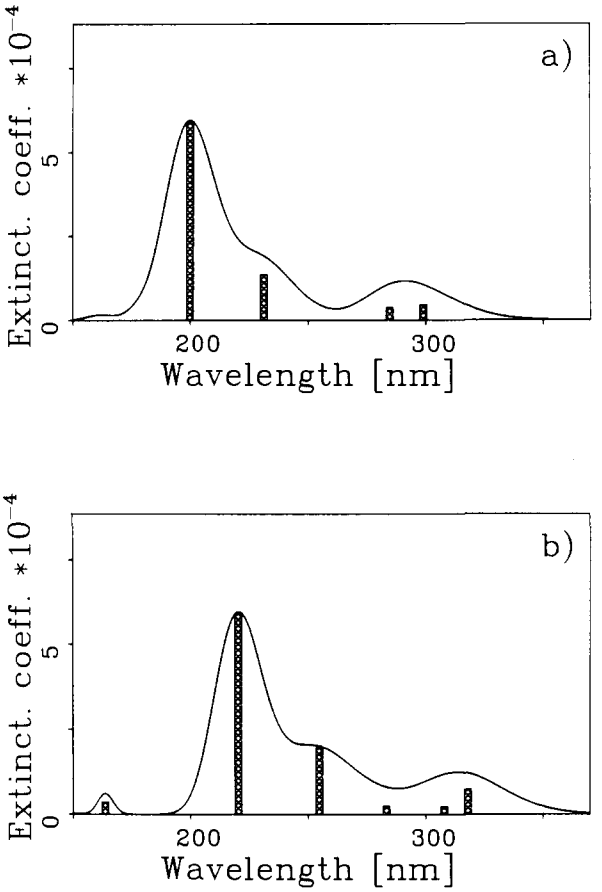

Figure 4. Simulated extinction coefficient ϵ (1 mol^{-1} cm^{-1}) of $Ni(CO)_4$. The bars represent the oscillator strength of the various transitions in arbitrary units, adjusted at the strongest single line. Note, ϵ (1 mol^{-1} cm^{-1}) = 2.61 × $10^{20}\sigma$ (cm^{-2}): (a) Full CIS calculation (energy broadening a_σ = 0.75 Å). (b) CISD calculation (energy broadening a_σ = 0.5 Å).

parametrization can be expected to compensate for multiple excitations if those configurations exhibit energies in the spectroscopic region of interest or if a given double excitation strongly mixes with the reference configuration. Double-excited CI calculations based on substitutions among the frontier orbitals have been performed in order to check the reliability of the CIS approximation for the present molecules and will be discussed below.

The CI calculations yield discrete energy levels for the electronic transitions. The experimental optical (or photoelectron) bands in most cases are broadened through vibronic interaction in the ground states[34] and direct dissociation in electronically excited states. To simulate such effects in an empirical fashion, we choose to convolute the line spectrum ϵ_i with a normalized Gaussian broadening resulting in a superposition of lines $g_i(\bar{\nu})$ weighted with the appropriate oscillator strength f_i

$$g_i(\bar{\nu}) = f_i[(2\pi)^{1/2}\sigma_i]^{-1} \exp[-(\bar{\nu} - \epsilon_i)^2/2\sigma_i^2] \quad (5)$$

where $\bar{\nu}$ is the transition frequency in wavenumbers and

$$\int g_i(\bar{\nu})\, d\bar{\nu} = f_i$$

Thus a more realistic presentation of the calculated spectra is achieved. Arguing from the Franck–Condon picture, one expects the number of involved vibronic states and, as a result, the broadening of any given transition to be related to the steepness of the final-state potential energy curve. Therefore, the broadening

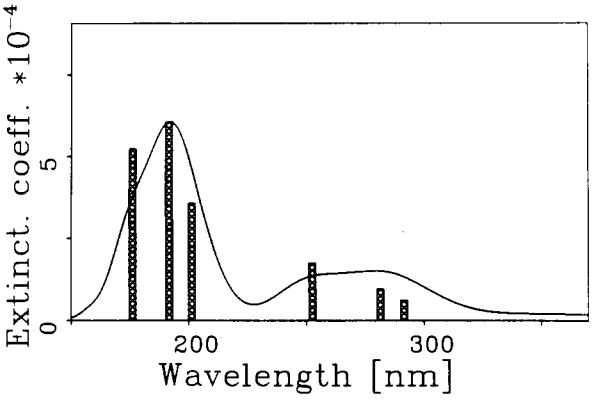

Figure 5. Calculated full CIS spectrum of $Fe(CO)_5$ (energy broadening a_σ = 1.0 Å). Layout as in Figure 4.

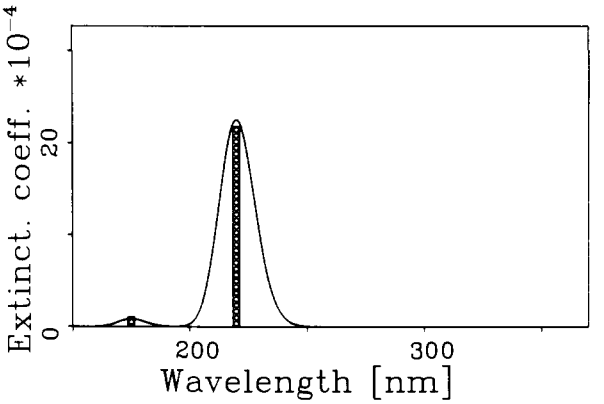

Figure 6. Calculated full CIS spectrum of $Cr(CO)_6$ (energy broadening a_σ = 0.5 Å). Layout as in Figure 4.

parameter σ_i of each transition is chosen proportional to the variation of the transition energy ϵ_i with the metal–ligand bond length b:

$$\sigma_i = a_\sigma \Delta\epsilon_i/\Delta b \quad (6)$$

The proportionality factor a_σ is chosen such that optimal similarity with the experimental spectrum is obtained. The corresponding values of a_σ are given with the graphical representation of the simulated spectra. Only the metal–ligand bond length variation is included in this scheme, because all important excitations in the spectroscopic region are of metal-to-ligand charge transfer type as will be shown subsequently.

The theoretical value f of the oscillator strength is related to the experimentally accessible extinction coefficient $\epsilon(\bar{\nu})$ (unit: 1 mol^{-1} cm^{-1}) via[7,34b]

$$f = (40\epsilon_0 mc^2 \ln 10/Le^2) \int \epsilon(\bar{\nu})\, d\bar{\nu}$$
$$= 4.315 \times 10^{-9} \int \epsilon(\bar{\nu})\, d\bar{\nu} \quad (7)$$

The simulated spectra in Figures 4–6 present the extinction coefficient ϵ as a superposition of broadened lines

$$\epsilon(\bar{\nu}) = g(\bar{\nu})/4.315 \times 10^{-9} \quad (8)$$

shown as a function of the wavelength to facilitate comparison with experimental data. As a check for our theoretical approach (including the line broadening), we note the fair agreement of the maximum of the extinction coefficient for $Ni(CO)_4$, $\epsilon_{max} \approx 6 \times 10^4$ (see Figure 4a), with the experimental value of 2.4 × 10^4.

Electronic Structure of the Metal Carbonyls

The electronic structure of the molecules under investigation is quite well-known.[38-47] It is nevertheless helpful to start our

(34) (a) Köppel, H.; Cederbaum, L. S.; Domcke, W.; Shaih, S. S. *Angew. Chem.* **1983**, *95*, 221. (b) Piepho, S. B.; Schatz, P. N. *Group Theory in Spectroscopy*; Wiley: New York, 1983; pp 6–26.
(35) Hedberg, L.; Iijima, T.; Hedberg, K. *J. Chem. Phys.* **1979**, *70*, 3224.
(36) Jones, L. H.; McDowell, R. S.; Goldblatt, M.; Swanson, B. I. *J. Chem. Phys.* **1972**, *57*, 2050.
(37) Rees, B.; Mitschler, A. *J. Am. Chem. Soc.* **1976**, *98*, 7918.
(38) Jörg, H.; Rösch, N. *Chem. Phys. Lett.* **1985**, *120*, 359.
(39) Rösch, N.; Jörg, H.; Dunlap, B. I. In *Quantum Chemistry: The Challenge of Transition Metals and Coordination Chemistry*; Veillard, A., Ed.; Reidel: Dordrecht, The Netherlands, 1986; p 179.

Table I. Experimental Bond Distances (in Å) Used in the Calculations

		M-C	C-O
$Ni(CO)_4$[a]		1.825	1.122
$Fe(CO)_5$[b]	axial	1.807	1.152
	equatorial	1.827	1.152
$Cr(CO)_6$[c]		1.915	1.140

[a] Reference 35. [b] Reference 36. [c] Reference 37.

discussion of the spectra by briefly reviewing those aspects of the electronic structure of these complexes that will influence the assignment of the spectra (e.g., ref 3). For each compound the experimental equilibrium geometry was used (Table I).

The generally accepted bonding mechanism of transition-metal carbonyls can be described as an interaction of CO 5σ-to-metal donation and metal-to-CO $2\pi^*$ back-donation. The importance of these contributions to the bond formation has been discussed previously.[38,41] It has been pointed out that the overall effect of CO σ donation is small since it may be characterized as interaction with the closed and spatially rather extended metal $n + 1$ s^2 shell. Therefore, the metal-to-CO back-donation is of increasing importance concomitant with the filling of the metal d levels.

In the case of nickel tetracarbonyl the metal 3d orbitals $9t_2$ and 2e are filled with 10 electrons and split into the characteristic ligand field pattern, t_2 above e, as a result of the CO 5σ-to-metal 3d interaction (see Table II). The orbital energies compare quite well with the experimental ionization potentials (IP_1 = 8.72 eV, IP_2 = 9.67 eV).[44] The corresponding σ-type orbitals of the CO ligands, $8t_2$ and $8a_1$, lie below the metal 3d orbitals. The $8t_2$ orbital is characterized as σ-bonding, in agreement with previous LCGTO-Xα calculations,[45] whereas Xα-SW[46] and other INDO-type[47] calculations characterize this orbital as predominantly π-bonding.

The occupied CO 1π orbitals $1t_1$, 1e, and $7t_2$ are not involved in the metal–ligand bonding. The lowest unoccupied molecular orbitals $10t_2$, 3e, and $2t_1$ result mainly from the ligand $2\pi^*$ orbitals. In contrast to other CNDO-type calculations,[3] where the $10t_2$ orbital exhibits a dominant metal p character, the lowest virtual t_2 orbital in the present calculation does not contain significant metal 4p contributions. This fact will be of importance for the characteristics of the spectrum (see below). Above the CO $2\pi^*$ orbitals lie the metal 4s ($9a_1$) and 4p ($11t_2$) orbitals.

In spite of the formal d occupation number of eight electrons, one finds the characteristic of the electronic structure of iron pentacarbonyl (Table III) very similar to that of nickel tetracarbonyl, with the exception of one unoccupied d level ($14a_1'$). Filled 5σ and 1π orbitals again lie below the filled metal d levels 10e′ and 3e″. The lowest unoccupied levels originate from CO $2\pi^*$ orbitals, just as in nickel tetracarbonyl, followed by levels with metal 3d, 4s, and 4p character at higher energy. The occupied orbital $13a_1'$ has a significant admixture of the metal d_{z^2} orbital in agreement with LCGTO-Xα calculations.[45] This is related to the fact that the Fe d_{z^2} orbital in iron pentacarbonyl is vacant and therefore available as an acceptor orbital. With an argument similar to the one given above for nickel tetracarbonyl,[38,41] one may rationalize the contribution of the Fe $3d_{z^2}$ orbital to ligand bonding. This preference is enforced by the resulting nodal structure of the $13a_1'$ orbital, which does not allow 4s admixture (see Figure 3a). As in nickel tetracarbonyl, the orbital energies of the occupied metal d levels are in good agreement with experimental ionization potentials (IP_1 = 8.6 eV, IP_2 = 9.9 eV).[48]

In the d^6 case of chromium hexacarbonyl, the correspondence between the one-electron levels, $\epsilon(2t_{2g})$ = 9.51 eV, $\epsilon(8t_{1u})$ = 14.13 eV, and $\epsilon(1t_{1g})$ = 15.06 eV, and low ionization potentials, IP_1 = 8.40 eV, IP_2 = 13.38 eV, and IP_3 = 14.21 eV,[49] is less satisfactory. Therefore, the value of the resonance parameter β_d(Cr) was changed from −26.0 eV[20] to −14.0 eV in order to achieve a better description of the nonpolar metal–carbon bond.[50] The resulting electronic structure of chromium hexacarbonyl is analogous to that of the metal carbonyls discussed above (see Table IV). The metal d levels are split in an occupied $2t_{2g}$ set and a vacant $6e_g$ level, which is available as acceptor orbital. The $2t_{2g}$ orbitals are stabilized by π back-donation, while the $6e_g$ level is destabilized by CO 5σ donation.

Spectra

$Ni(CO)_4$. The solution spectrum of nickel tetracarbonyl, known for quite some time,[2] exhibits three main peaks at energies of 6.0, 5.5, and 5.2 eV. A matrix isolation spectrum[51] shows only the strongest absorption at 5.2 eV and a shoulder at 4.5 eV. The bands were classified as metal-to-ligand charge-transfer (MLCT) excitations of the type M e, t_2 to L π^* and M t_2 to L π^*.[51] In the experimental UV spectrum presented here, a main peak at 207 nm (6.0 eV) ($\epsilon = 2.4 \times 10^5$) and two shoulders at 230 nm (5.4 eV) and 270 nm (4.6 eV) can be discriminated (see Figure 1).

The results of the full CIS procedure are listed in Table V. This calculation yields excitation energies and oscillator strengths essentially in the correct range. The spectrum is dominated by MLCT excitations from the metal 3d orbitals into the vacant $2\pi^*$ orbitals of the ligands. Metal d–s and d–p transitions are not associated with significant oscillator strength and therefore play a minor role in the interpretation of the experimental spectrum. This is in contrast to previous CNDO CI calculations[3] where the d–p excitation lies in the energy range of the spectrum and exhibits considerable oscillator strength.

Two transitions may be assigned easily. We attribute the strongest transition at 6.0 eV to the $6T_2$ state calculated at 6.2 eV with the highest oscillator strength in the spectral region. This transition is dominated by a 2e → $2t_1$ (d → $2\pi^*$) MLCT-type excitation. The shoulder at 5.4 eV we assign to the transition $1A_1$ → $5T_2$ calculated at 5.36 eV. The broad shoulder near 4.6 eV should be related to all T_2 states, from $1T_2$ to $4T_2$. In this interpretation of the spectrum all important transitions are of M d → L π^* charge-transfer character. The INDO/S calculation reproduces very well both the energies and the relative oscillator strengths of these transitions. Symmetry- or spin-forbidden transitions may borrow intensity by vibronic or spin–orbit coupling[7] thus broadening the spectrum (see Figures 1 and 4). The smoothing of the line spectrum via the convolution technique described above yields a rather satisfactory agreement between experimental and theoretical spectra.

Six low-lying spin-forbidden singlet–triplet transitions of M d → L π^* charge-transfer character are calculated in the energy range from 3.36 to 3.94 eV. They arise from the substitutions $9t_2$ → $10t_2$ (A_1, E, T_1, T_2) and $9t_2$ → 3e (T_1, T_2). The first singlet–triplet metal-to-metal transition, calculated at an energy of 4.06 eV (1^1A_1 → 3^3T_2), is of the type M d → M s.

To investigate the effect of double substitutions, the number of single excitations had to be reduced for storage reasons. A CIS was performed as new reference, with molecular orbitals of types

(40) Baerends, E. J.; Rozendaal, A. In *Quantum Chemistry: The Challenge of Transition Metals and Coordination Chemistry*; Veillard, A., Ed.; Reidel: Dordrecht, The Netherlands, 1986; p 159.
(41) (a) Bauschlicher, C. W.; Bagus, P. S. *J. Chem. Phys.* **1984**, *81*, 5889. (b) Bauschlicher, C. W.; Langhoff, S. R.; Barnes, L. A. *Chem. Phys.* **1989**, *129*, 431.
(42) Baerends, E. J.; Ros, P. *Mol. Phys.* **1975**, *30*, 1735.
(43) Weber, J.; Geoffroy, M.; Goursot, A.; Peningault, E. *J. Am. Chem. Soc.* **1978**, *100*, 3995.
(44) Reutt, E.; Wang, L. S.; Shirley, D. A. *Chem. Phys. Lett.* **1986**, *126*, 399.
(45) Rösch, N.; Jörg, H.; Kotzian, M. *J. Chem. Phys.* **1987**, *86*, 4038.
(46) Howard, I. A.; Pratt, G. W.; Johnson, K. H.; Dresselhaus, G. *J. Chem. Phys.* **1981**, *74*, 3415.
(47) Ziegler, T. *Acta Chem. Scand.* **1974**, *28A*, 29.
(48) Baerends, E. J.; Oudshoorn, C.; Oskam, A. *J. Electron Spectrosc. Relat. Phenom.* **1975**, *6*, 259.
(49) Higginson, B. R.; Lloyd, D. R.; Burroughs, P.; Gibson, D. M.; Orchard, A. F. *J. Chem. Soc., Faraday Trans.* **1973**, *69*, 1659.
(50) The effect of changing β values for these compounds is very slight as can be seen from a variation from −26 to −14 eV changing the values of the frontier orbitals an average of less than 1 eV. The β values of the original INDO work were fit to metal complexes with 2+/3+ valence states, and it is easily shown that β values should increase for zerovalent state complexes such as these.
(51) Lever, A. B. P.; Ozin, G. A.; Hanlan, A. J.; Power, W. J.; Gray, H. B. *Inorg. Chem.* **1970**, *18*, 2088.

Table II. Orbitals of $Ni(CO)_4$ and Their Mulliken Populations

orbital energy, eV	orbital type		Mulliken populations, %						
			Ni			C		O	
			4s	4p	3d	2s	2p	2s	2p
11.96	$12t_2$	L 6σ		11.4	1.1	4.0	49.4	9.8	24.2
10.43	$10a_1$	L 6σ	4.9			9.2	45.5	11.4	29.1
4.59	$11t_2$	M 4p		69.7	0.3	16.4	7.4	1.4	4.8
2.02	$9a_1$	M 4s	76.7			20.1	0.5	0.6	2.3
0.57	$2t_1$	L 2π					75.2		24.8
0.40	3e	L 2π			16.7		65.9		23.4
0.25	$10t_2$	L 2π		1.3	10.3	5.6	59.3	0.3	23.3
−9.15[a]	$9t_2$	M 3d		6.4	70.6	2.9	6.1	0.3	23.3
−10.06[a]	2e	M 3d			85.0		2.6		12.4
−15.39	$8t_2$	L 5σ		1.9	15.7	11.9	28.6	2.1	39.9
−15.68	$1t_1$	L 1π					24.8		75.2
−16.40	1e	L 1π			4.3		31.5		64.2
−16.65	$7t_2$	L 1π		2.8	0.1	1.2	32.2	3.6	60.1
−17.44	$8a_1$	L 5σ	2.6			0.2	22.4	17.3	57.5
−20.24	$6t_2$	L 4σ		5.7	1.8	37.2	4.7	23.7	26.9
−23.14	$7a_1$	L 4σ	14.4			48.2	20.2	12.8	4.3
−44.63	$5t_2$	L 3σ		0.9	0.0	20.8	12.3	59.1	6.8
−44.87	$6a_1$	L 3σ	1.4			22.3	11.5	58.1	6.8

[a] Assuming the frozen orbital approximation, these values might be compared with observed ionization[44] potentials of 8.72 and 9.67 eV. A consistent relaxation energy of 0.4 eV is implied.

Table III. Orbitals of $Fe(CO)_5$ and Their Mulliken Populations[a]

orbital energy, eV	orbital type		Mulliken populations, %						
			Fe			C		O	
			4s	4p	3d	2s	2p	2s	2p
3.46	$10a_2''$	M 4p		71.8		17.8	6.1	0.7	3.6
3.32	13e′	M 4p		71.5	0.6	16.1	7.7	0.6	3.5
1.18	8e″	L 2π			0.2		80.0		19.8
1.14	$15a_1'$	M 4s	76.5		1.8	19.3	0.5	0.1	1.7
0.52	$14a_1'$	M 3d	2.2		60.9	25.5	2.4	1.1	7.8
0.37	12e′	L 2π		0.4	21.9	5.0	54.1	0.2	18.6
0.05	$9a_2''$	L 2π		0.9		8.2	66.4	0.3	24.2
−0.29	4e″	L 2π			25.2		53.8		21.0
−0.31	$2a_2'$	L 2π					74.1		25.9
−0.32	11e′	L 2π		0.1	0.5	4.3	69.9	0.1	25.0
−9.01[b]	10e′	M 3d		7.2	58.3	1.1	8.5	0.0	23.7
−10.33[b]	3e″	M 3d			66.0		4.9		29.0
−14.06	$8a_2''$	L 5σ		2.7		9.7	20.6	0.4	66.6
−14.81	9e′	L 5σ		1.2	6.7	7.7	22.3	0.7	61.3
−14.88	$13a_1'$	L 5σ	0.3		29.7	24.7	27.7	1.2	16.4
−14.98	2e″	L 1π			0.0		19.9		80.1
−15.51	$1a_2'$	L 1π					25.9		74.1
−16.10	8e′	L 1π		0.1	7.1	1.0	31.2	0.3	60.4
−17.16	7e′	L 1π		2.2	0.9	0.2	29.9	10.3	56.5
−17.32	$7a_2''$	L 1π		1.9		0.1	29.5	11.9	56.6
−17.39	1e″	L 1π			8.6		41.3		50.1
−17.86	$12a_1'$	L 5σ	0.8		0.3	0.5	18.1	21.9	58.4

[a] 3σ, 4σ, and 6σ derived molecular orbitals not shown for clarity. [b] Ionization potentials are observed[48] at 8.6 and 9.9 eV, implying a 0.4 eV relaxation energy (see Table II, footnote *a*).

3σ, 4σ, and 6σ being excluded. The calculated transition energies changed by less than 0.05 eV and the oscillator strengths by less than 10% in comparison with the full CIS case. Double substitutions from the occupied metal orbitals ($2e$, $9t_2$) into the vacant CO $2\pi^*$ levels ($10t_2$, $3e$, $2t_1$) were then added to the single-substituted determinants. On the basis of this single–double CI (CISD) calculation, the details of which are not given here, one may deduce that doubly excited configurations do not significantly influence the characteristics of the spectrum (see Figure 4b) and that no double excitations fall into the relevant spectral region. A small shift of oscillator strength was observed though, between the states $4T_2$ and $5T_2$ with the result that the CISD calculation resembles the experimental spectrum somewhat better.

$Fe(CO)_5$. The UV spectrum of iron pentacarbonyl (see Figure 1) exhibits two main bands with maxima at about 245 nm (5.0 eV) and probably lower than 200 nm (>6.2 eV). In the solvent spectrum[5] an additional band at 280 nm (4.4 eV) with about one-third of the oscillator strength of the transition at 5.0 eV was found. The soft ascent in the low-energy region of the present spectrum can be interpreted as a shoulder, but the location of the center of energy is not clear.

All excitations in the calculated spectrum (see Table VI and Figure 5) result from transitions starting from the metal 3d orbitals 10e′ and 3e″. The lowest excitation is the M d → M d transition $10e' \rightarrow 14a_1'$, which is Laporte forbidden and thus does not carry any oscillator strength. As in nickel tetracarbonyl, the spectrum is dominated by MLCT transitions. M d → M s transitions are observed at 4.25 and 5.51 eV and M d → M p excitations at an energy of 6.36 eV and higher. A previously published CNDO CI calculation[3] is in essential agreement with these results but is shifted to higher energy compared with our spectrum and the experimental spectrum.

All excitations in the region between 5.73 and 6.48 eV, with the transitions $3e'' \rightarrow 11e'$ and $3e'' \rightarrow 9a_2''$ contributing strongest to the oscillator strength, may be assigned to the main band in the experimental spectrum. The maximum of the calculated band is found at an energy higher than 6.2 eV in agreement with trends extrapolated from the experimental spectrum near 200 nm (see

Table IV. Orbitals of $Cr(CO)_6$ and Their Mulliken Populations[a]

orbital energy, eV	orbital type		Mulliken populations, %						
			Cr			C		O	
			4s	4p	3d	2s	2p	2s	2p
3.13	$10t_{1u}$	M 4p		72.3		16.7	7.3	0.5	3.2
1.26	$2t_{1g}$	L 2π					79.1		20.9
1.18	$6e_g$	M 3d			66.6	23.9	1.4	1.2	6.9
0.98	$9a_{1g}$	M 4s	78.7			19.3		0.1	1.4
0.63	$3t_{2g}$	L 2π			38.5		47.2		14.3
−0.15	$2t_{2u}$	L 2π					73.6		26.4
−0.22	$9t_{1u}$	L 2π		1.7		8.6	64.1	0.2	25.4
−8.95[b]	$2t_{2g}$	M 3d			53.7		11.2		35.1
−14.14[b]	$8t_{1u}$	L 5σ		3.1		10.4	22.1	0.5	63.9
−14.73	$5e_g$	L 5σ			23.1	19.4	30.5	2.7	24.3
−15.06[b]	$1t_{1g}$	L 1π					20.9		79.1
−15.63	$1t_{2u}$	L 1π					26.4		73.6
−17.24	$7t_{1u}$	L 1π		1.8			27.9	12.3	58.0
−17.28	$1t_{2g}$	L 1π			7.9		41.6		50.6
−17.76	$8a_{1g}$	L 5σ	0.8			0.5	17.3	22.1	59.3

[a] Results for $\beta_d(Cr) = -14.0$ eV. 3σ, 4σ, and 6σ derived molecular orbitals not shown for clarity. [b] For comparison, ionization potentials are observed[49] at 8.40, 13.38, and 14.21 eV, implying a relaxation energy of about 0.6 eV.

Table V. Low-Energy Part of Full Single Excitation CI of $Ni(CO)_4$

energy					
in eV	in nm	oscill strength	final state[a]	character	comptn of final state[b]
3.93	316	0.0	$1T_1$	M d → L π^*	97% $9t_2 \rightarrow 10t_2$
3.98	312	0.0	1E	M d → L π^*	91% $9t_2 \rightarrow 10t_2$
4.05	306	0.0	$2T_1$	M d → L π^*	97% $9t_2 \rightarrow 3e$
4.15	299	0.136	$1T_2$	M d → L π^*	78% $9t_2 \rightarrow 10t_2$, 16% $9t_2 \rightarrow 9a_1$
4.36	285	0.111	$2T_2$	M d → L π^*	86% $9t_2 \rightarrow 3e$
4.39	283	0.001	$3T_2$	M d → M s	77% $9t_2 \rightarrow 9a_1$, 13% $9t_2 \rightarrow 10t_2$
4.55	272	0.0	$3T_1$	M d → L π^*	73% $2e \rightarrow 10t_2$, 25% $9t_2 \rightarrow 2t_1$
4.56	272	0.0	$2A_1$	M d → L π^*	57% $9t_2 \rightarrow 10t_2$, 41% $2e \rightarrow 3e$
4.64	268	0.0	$1A_2$	M d → L π^*	64% $9t_2 \rightarrow 2t_1$, 35% $2e \rightarrow 3e$
4.79	259	0.0	2E	M d → L π^*	89% $9t_2 \rightarrow 2t_1$
4.91	252	0.021	$4T_2$	M d → L π^*	81% $2e \rightarrow 10t_2$, 15% $9t_2 \rightarrow 2t_1$
4.92	252	0.0	$4T_1$	M d → L π^*	74% $9t_2 \rightarrow 2t_1$, 24% $2e \rightarrow 10t_2$
4.95	251	0.0	3E	M d → M s	95% $2e \rightarrow 9a_1$
5.11	243	0.0	$2A_2$	M d → L π^*	65% $2e \rightarrow 3e$, 35% $9t_2 \rightarrow 2t_1$
5.29	234	0.0	4E	M d → L π^*	82% $2e \rightarrow 3e$
5.36	231	0.446	$5T_2$	M d → L π^*	56% $9t_2 \rightarrow 2t_1$, 26% $2e \rightarrow 2t_1$
5.71	217	0.0	$5T_1$	M d → L π^*	97% $2e \rightarrow 2t_1$
6.20	200	1.737	$6T_2$	M d → L π^*	70% $2e \rightarrow 2t_1$, 13% $9t_2 \rightarrow 2t_1$
6.88	180	0.0	$6T_1$	M d → M p	95% $9t_2 \rightarrow 11t_2$

[a] Only singlet states are listed. [b] Only contributions of formal transitions with a weight of 10% or higher are shown.

Figure 1). The maximum in the solvent spectrum[5] at 6.3 eV falls between the states 7E′ (x, y) and $4A_2''$ (z) at 6.16 and 6.47 eV. The band near 250 nm (5.0 eV) in the spectrum (see Figure 1) may be assigned to the calculated transition 3e″ → 4e″ (6E′) at an energy of 4.91 eV. According to the present calculations, the two excitations $1A_1' \rightarrow 3E'$ (4.25 eV) and $1A_1' \rightarrow 5E'$ (4.41 eV) are responsible for the soft ascent in the low-energy region of the spectrum. The transition probability into the state 3E′ results mainly from the CT transition 10e′ → 11e′.

The d–d excitations (10e′ → $14a_1'$ and 3e″ → $14a_1'$) are calculated at energies of 2.89 and 3.60 eV, respectively. In the solvent spectrum[5] the band at 4.4 eV has been interpreted as a d–d transition, because it was found to be not very sensitive to a change of the temperature (300 vs 77 K). According to our calculations, the two transitions $1A_1' \rightarrow 3E'$ and $1A_1' \rightarrow 5E'$ furnish the main contributions to this band. The oscillator strengths thereby result from charge-transfer excitations, but a very significant admixture to the wavefunction, especially in the transition $1A_1' \rightarrow 3E'$, originates from M d → M s substitution. The latter characteristics correlate well with the observed low sensitivity of the band to change in temperature.

The first calculated triplet state $1^3E'$ at 2.22 eV results from the d–d excitation 10e′ → $14a_1'$ and lies about 0.7 eV lower than the corresponding singlet state $1^1E'$. Two further low-lying triplet states ($1^3A_1''$, $1^3E''$) calculated at energies of 2.84 and 2.95 eV, originate from the charge-transfer excitation 10e′ → 4e″.

$Cr(CO)_6$. The UV spectrum of chromium hexacarbonyl (Figure 1) exhibits two bands at 227 nm (5.5 eV) and 280 nm (4.4 eV). A vapor spectrum[4] shows also two main peaks located at energies of 225 nm (5.48 eV) and 390 nm (4.44 eV) with an intensity ratio of 9:1.

The calculated spectrum of chromium hexacarbonyl is presented in Table VII and Figure 6. The lowest excitation is calculated to be of M d → M d type, and the spectral region is dominated by MLCT transitions. At energies higher than 6.9 eV M d → M p transitions are found, and the only M d → M s transition is at an energy of 4.77 eV. The energies of the d–d excitations ($2t_{2g} \rightarrow 6e_g$) calculated at 3.64 eV ($1T_{1g}$) and 4.14 eV ($1T_{2g}$) are in good agreement with the corresponding experimental values[4] of 3.6 and 3.9 eV. The two spin-forbidden and Laporte forbidden M d → M d transitions $1^1A_{1g} \rightarrow 1^3T_{1g}$ and $1^1A_{1g} \rightarrow 1^3T_{2g}$ are calculated about 0.4 eV lower than the corresponding singlet–singlet transitions. In the energy range between 3.33 and 3.98 eV the charge-transfer states 1^3A_{1g}, 1^3E_g, and 2^3T_{2g} are calculated, resulting from the substitution $2t_{2g} \rightarrow 3t_{2g}$.

Within these calculations the excitations $1A_{1g} \rightarrow 1T_{1u}$ and $1A_{1g} \rightarrow 2T_{1u}$ are without doubt responsible for the two experimental bands but with extremely disparate intensity (400:1). The question then arises as to what is the reason for this large discrepancy with the experiment. The two excitations are combinations of the same two transitions, $2t_{2g} \rightarrow 9t_{1u}$ and $2t_{2g} \rightarrow 2t_{2u}$, with almost equal composition that differ in sign only. The pure transitions $2t_{2g} \rightarrow$

Table VI. Low-Energy Part of Full Single Excitation CI of $Fe(CO)_5$

energy in eV	energy in nm	oscill strength	final state[a]	character	comptn of final state[b]
2.89	430	0.0	1E′	M d → M d	91% 10e′ → 14a_1′
3.01	412	0.0	1A_1″	M d → L π*	98% 10e′ → 4e″
3.28	378	0.0	1E″	M d → L π*	92% 10e′ → 4e″
3.44	361	0.039	1A_2″	M d → L π*	98% 10e′ → 4e″
3.60	345	0.0	2E″	M d → M d	93% 3e″ → 14a_1′
3.78	328	0.0	1A_2′	M d → L π*	65% 10e′ → 12e′, 32% 10e′ → 11e′
3.92	317	0.025	2E′	M d → L π*	44% 10e′ → 11e′, 43% 10e′ → 12e′
4.13	300	0.0	2A_2′	M d → L π*	47% 10e′ → 11e′, 26% 3e″ → 4e″ 25% 10e′ → 12e′
4.25	292	0.104	3E′	M d → M s	57% 10e′ → 15a_1′, 30% 10e′ → 11e′
4.27	291	0.019	4E′	M d → L π*	40% 10e′ → 2a_2′, 23% 10e′ → 15a_1′ 17% 10e′ → 12e′
4.30	288	0.0	3E″	M d → L π*	90% 10e′ → 9a_2″
4.35	285	0.0	2A_1′	M d → L π*	39% 10e′ → 12e′, 30% 3e″ → 4e″ 29% 10e′ → 11e′
4.41	281	0.161	5E′	M d → L π*	31% 10e′ → 2a_2′, 17% 10e′ → 12e′ 16% 3e″ → 4e″, 12% 10e′ → 15a_1′
4.51	275	0.0	3A_1′	M d → L π*	68% 10e′ → 11e′, 19% 10e′ → 12e′
4.54	273	0.0	3A_2′	M d → L π*	71% 3e″ → 4e″, 19% 10e′ → 11e′
4.91	253	0.296	6E′	M d → L π*	67% 3e″ → 4e″, 14% 10e′ → 2a_2′
4.94	251	0.0	2A_1″	M d → L π*	47% 3e″ → 11e′, 38% 3e″ → 12e′
5.09	244	0.0	3A_1″	M d → L π*	58% 3e″ → 12e′, 21% 3e″ → 11e′ 19% 10e′ → 5e″
5.09	243	0.0	4E″	M d → L π*	74% 3e″ → 11e′, 13% 3e″ → 12e′
5.21	238	0.0	5E″	M d → L π*	56% 3e″ → 2a_2′, 28% 3e″ → 12e′
5.35	232	0.027	2A_2″	M d → L π*	94% 3e″ → 12e′
5.44	228	0.0	4A_1″	M d → L π*	67% 10e′ → 5e″, 29% 3e″ → 11e′
5.51	225	0.0	6E″	M d → M s	88% 3e″ → 15a_1′
5.56	223	0.0	7E″	M d → L π*	75% 10e′ → 5e″
5.72	217	0.0	8E″	M d → L π*	43% 3e″ → 12e′, 27% 3e″ → 2a_2′
5.73	216	0.002	2A_2″	M d → L π*	84% 10e′ → 5e″, 11% 3e′ → 11e′
6.16	201	0.610	7E′	M d → L π*	79% 3e″ → 9a_2″
6.36	195	0.0	4A_2′	M d → M p	96% 10e′ → 13e′
6.47	192	1.037	4A_2″	M d → L π*	79% 3e″ → 11e′, 12% 10e′ → 5e″
6.48	191	0.016	8E′	M d → M p	92% 10e′ → 13e′
6.53	190	0.0	4A_1′	M d → M p	92% 10e′ → 13e′

[a] Only singlet states are listed. [b] Only contributions of formal transitions with a weight of 10% or higher are shown.

Table VII. Low-Energy Part of Full Single Excitation CI of $Cr(CO)_6$[a]

energy in eV	energy in nm	oscill strength	final state[b]	character	comptn of final state[c]
3.64	340	0.0	$1T_{1g}$	M d → M d	94% $2t_{2g}$ → $6e_g$
4.14	300	0.0	$1T_{2g}$	M d → M d	57% $2t_{2g}$ → $6e_g$, 42% $2t_{2g}$ → $3t_{2g}$
4.16	298	0.0	$1E_u$	M d → L π*	89% $2t_{2g}$ → $9t_{1u}$
4.19	296	0.0	$1A_{1u}$	M d → L π*	99% $2t_{2g}$ → $2t_{2u}$
4.21	294	0.0	$1T_{2u}$	M d → L π*	63% $2t_{2g}$ → $9t_{1u}$, 36% $2t_{2g}$ → $2t_{2u}$
4.21	294	0.0	$1A_{2u}$	M d → L π*	99% $2t_{2g}$ → $9t_{1u}$
4.25	292	0.0	$2E_u$	M d → L π*	90% $2t_{2g}$ → $2t_{2u}$
4.32	287	0.0	$2T_{1g}$	M d → L π*	93% $2t_{2g}$ → $3t_{2g}$
4.57	272	0.0	$1E_g$	M d → L π*	94% $2t_{2g}$ → $3t_{2g}$
4.60	269	0.010	$1T_{1u}$	M d → L π*	59% $2t_{2g}$ → $9t_{1u}$, 41% $2t_{2g}$ → $2t_{2u}$
4.62	269	0.0	$2T_{2u}$	M d → L π*	63% $2t_{2g}$ → $2t_{2u}$, 36% $2t_{2g}$ → $9t_{1u}$
4.77	260	0.0	$2T_{2g}$	M d → M s	77% $2t_{2g}$ → $9a_{1g}$, 12% $2t_{2g}$ → $3t_{2g}$
4.99	249	0.0	$3T_{2g}$	M d → L π*	42% $2t_{2g}$ → $3t_{2g}$, 32% $2t_{2g}$ → $6e_g$ 23% $2t_{2g}$ → $9a_{1g}$
5.60	221	0.0	$1A_{2g}$	M d → L π*	97% $2t_{2g}$ → $2t_{1g}$
5.79	214	3.993	$2T_{1u}$	M d → L π*	56% $2t_{2g}$ → $2t_{2u}$, 36% $2t_{2g}$ → $9t_{1u}$
5.81	213	0.0	$3T_{1g}$	M d → L π*	96% $2t_{2g}$ → $2t_{1g}$
5.85	212	0.0	$4T_{2g}$	M d → L π*	96% $2t_{2g}$ → $2t_{1g}$
6.64	187	0.0	$2E_g$	M d → L π*	93% $2t_{2g}$ → $2t_{1g}$
6.91	180	0.0	$2A_{2u}$	M d → M p	99% $2t_{2g}$ → $10t_{1u}$
6.92	179	0.0	$3T_{2u}$	M d → M p	99% $2t_{2g}$ → $10t_{1u}$
7.06	176	0.0	$3E_u$	M d → M p	99% $2t_{2g}$ → $10t_{1u}$
7.13	174	0.175	$3T_{1u}$	M d → M p	94% $2t_{2g}$ → $10t_{1u}$
7.22	172	0.0	$2A_{1g}$	M d → L π*	70% $2t_{2g}$ → $3t_{2g}$, 27% $5e_g$ → $6e_g$

[a] Results obtained for $\beta_d(Cr) = -14.0$ eV. [b] Only singlet states are listed. [c] Only contributions of formal transitions with a weight of 10% or higher are shown.

$9t_{1u}$ and $2t_{2g} \rightarrow 2t_{2u}$ have rather similar transition moments, again with opposite sign (+4.474, −4.861 au, respectively). The resulting oscillator strengths in the CI states $1T_{1u}$ and $2T_{1u}$ are a squared linear combination of the transition moments of the pure transitions. Depending on the sign of the linear combination of the relevant determinants, there can be reinforcement ($2T_{1u}$) or near

Table VIII. Orbital Energy Levels in Chromium Carbonyl Complexes[a]

molecule	metal d levels			CO 2π levels[b]					
$Cr(CO)_6$		$2t_{2g}$			$9t_{1u}$			$2t_{2u}$	
		−8.95			−0.22			−0.15	
$(CO)_5CrCS$	$2b_2$	13e		14e	$24a_1$		15e	$7b_1$	
	−9.13	−8.86		−1.27	−0.60		−0.44	−0.41	
$(CO)_5Cr(PF_3)$	20a″	47a′	21a″	48a′	22a″	49a′	50a′	23a″	51a′
	−8.88	−8.82		−0.50	−0.04		0.01	0.77	
$(CO)_5Cr(CHOH)$	20a″	47a′	21a″	48a′	22a″	49a′	50a′	23a″	51a′
	−8.67	−8.66	−8.43	0.10	0.16	0.17	0.18	0.85	1.06

[a] Energies in electronvolts. [b] Only those CO 2π orbitals are listed that correspond to the $9t_{1u}$ and $2t_{2u}$ orbitals in $Cr(CO)_6$.

canceling of the transition moments ($1T_{1u}$).

The calculated oscillator strength of these two bands is thus a sensitive function of the mixing of these two determinants with nearly equal oscillator strength. This mixing, in turn, depends on the energy separation of the two relevant orbitals $9t_{1u}$ and $2t_{2u}$ and on the nature of higher excited configurations, which mix through the CI, again influencing the combination of the two most important determinants. For example, the interligand CO–CO interaction is of π character in both orbitals, but it is bonding in the $9t_{1u}$ orbital, while it is antibonding in the $2t_{2u}$ orbital (see Figures 3b and 3c). The latter molecular orbital is thus expected to be more sensitive to a variation of the metal–ligand bond length and, consequently, of the interligand distance. Elongating the Cr–C distance by 0.1 Å decreases the ratio to 170:1 while a shortening increases it to 3400:1. The suggested critical dependence of the two final states on the ligand–ligand interaction may be confirmed in another computer experiment by increasing the weight factor $f_{p\pi}$ (eq 4) of the π component of the overlap in the two-center Fock matrix elements simulating a somewhat stronger metal-to-ligand π interaction. Choosing a higher weight for the π overlap ($f_{p\pi} = 0.800$) increases the energy difference of the $9t_{1u}$ and $2t_{2u}$ from 0.07 to 0.52 eV and reduces the ratio of the oscillator strengths to 11:1, in good agreement with experiment.

We have also examined the influence of double-excited states on the relative intensity of these two allowed transitions. Briefly, higher excited configurations in the CI treatment try to depress the higher of the two calculated transitions. This depression is strongly "resisted" by the lower lying one of the pair, changing the mixing between the pair, and redistributing the oscillator strength.[52] In the case of chromium hexacarbonyl, the $2T_{1u}$ state is depressed by 0.16 eV, while the $1T_{1u}$ state is shifted by 0.21 eV to higher energy. Redistribution of oscillator strength due to the change in mixing increases the ratio of the oscillator strengths in this case to 2500:1, consistent with the effect of metal–carbon bond elongation on changes in excitation energies and oscillator strengths.

These results for chromium hexacarbonyl have spawned further investigations in order to elaborate on the disparate mixing of the two excitations by substituting one carbon monoxide ligand by various other ligands and thus reducing the symmetry of the chromium carbonyl compound.

$(CO)_5CrCS$. In the first step the closed-shell molecule CS was introduced, leading to a complex $(CO)_5CrCS$ with C_{4v} symmetry. Hereby the original metal d level $2t_{2g}$ of $Cr(CO)_6$ splits in the orbitals 13e and $2b_2$, separated by 0.27 eV (see Table VIII). The $9t_{1u}$ orbitals of $Cr(CO)_6$ correlate with 14e and $24a_1$ and the $2t_{2u}$ orbitals with 15e and $7b_1$ in $(CO)_5CrCS$. The orbital $24a_1$ may be related to the corresponding z component of a t_{1u}-like orbital and the orbital $7b_1$ to the $z(x^2 - y^2)$ component of a t_{2u}-like orbital, while the e orbitals are a plus (14e) and minus (15e) linear combination of $9t_{1u}$ and $2t_{2u}$. In analogy to $Cr(CO)_6$ the pure excitations $13e \rightarrow 24a_1$ and $13e \rightarrow 7b_1$ are accompanied with comparable oscillator strength (0.328, 0.527), whereas the transitions into the orbitals 14e and 15e exhibit extremely disparate oscillator strength ($13e \rightarrow 14e$, 1.82; $13e \rightarrow 15e$, 0.01; $2b_2 \rightarrow 14e$, 0.00; $2b_2 \rightarrow 15e$, 1.69), a fact which is due to the linear combination of determinants discussed above.

The calculated spectrum of $(CO)_5CrCS$ exhibits three main peaks at 5.88, 4.80, and 4.42 eV (intensity ratio 2.5:0.7:1). But in this case the most intense transition has no determinant in common with the other two. Experimentally one finds two strong bands located at 5.4 eV (228 nm) and 4.3 eV (291 nm), the latter with a shoulder at 4.5 eV (275 nm) and both with nearly equal extinction coefficient.[53] It is gratifying to note that in this case with apparently no critical determinantal superposition the agreement between experimental and calculated intensity distribution over the two major bands is much improved.[53]

$(CO)_5Cr(PF_3)$. The complex $(CO)_5Cr(PF_3)$ has C_s symmetry. Bond lengths were estimated from crystal data available for triphenylphosphine and triphenyl phosphite substituted pentacarbonylchromium compounds.[54] When the metal and ligand orbitals are analyzed, the local symmetry of the $(CO)_5Cr$ fragment is not much disturbed by the PF_3 ligand. The orbitals (47a′, 21a″), (22a″, 49a′), and (23a″, 51a′) can be compared with the corresponding e orbitals of $(CO)_5CrCS$ (see Table VIII). The contributions of the PF_3 ligand orbitals are small. In the calculated spectrum the most intense transitions found at energies of 5.92 eV (16A′, 21A″) and 6.46 eV (17A′) are comparable to excitations into the state $2T_{1u}$ (5.79 eV) of $Cr(CO)_6$. The excitations related to the transition $1A_{1g} \rightarrow 1T_{1u}$ (4.60 eV) of $Cr(CO)_6$ are calculated at energies of 4.69 eV (10A′, 13A″) and 4.70 eV (11A′). These groups of transitions carry oscillator strengths according to the ratio of about 230:1, which reduces to 18:1 when a value of 0.800 is chosen for the empirical parameter $f_{p\pi}$ (see above).

$(CO)_5CrC(OH)H$. Structural data for the model carbene $(CO)_5CrC(OH)H$ (C_s symmetry) were estimated from crystal data of various pentacarbonylchromium carbene complexes.[55] In spite of the fact that in this case the local C_{4v} symmetry of the $(CO)_5Cr$ fragment is broken by the carbene ligand (see Table VIII), the most intense electronic transitions are comparable to that of the PF_3-substituted carbonyl compound. The transitions are calculated at energies of 5.90 eV (19A′), 5.91 eV (21A″), and 6.45 eV (21A′). The states analogous to $1T_{1u}$ are spread over a range of about 0.6 eV in the spectrum of the carbene compound, rendering the separation into the two relevant groups somewhat uncertain. A ratio of 190:1 has been calculated for the oscillator strengths (20:1 for $f_{p\pi} = 0.800$). No experimental data concerning relative transition probabilities were available to us. The transition energies for the lowest charge-transfer and for one d–d excitation are known for several pentacarbonylchromium carbene complexes.[56] The calculated transition energies of 406 nm (charge transfer) and 349 nm (d–d) of our model carbene complex are in satisfactory agreement with the experimental energies of about 380 nm (MLCT) and 320 nm (d–d), the values varying slightly with the nature of the carbene substituents.[56]

The studies of the various carbonylchromium complexes show that the highly disparate ratio of oscillator strength of the two transitions $1A_{1g} \rightarrow 1T_{1u}$ and $1A_{1g} \rightarrow 2T_{1u}$ in $Cr(CO)_6$ is not just

(52) Both of these effects on calculated oscillator strength distributed between two states composed of two determinants of near equal oscillator strength are well documented. See, for example: Edwards, W. D.; Weiner, B.; Zerner, M. C. *J. Am. Chem. Soc.* **1986**, *108*, 2196. In this case, (porphinato)iron(II), the nearly degenerate orbitals are the occupied ones, as opposed to the virtual ones.

(53) Baibich, I. M.; Butler, I. S. *Inorg. Chim. Acta* **1984**, *89*, 73.

(54) Plastas, J. H.; Stewart, J. M., Grim, S. O. *Inorg. Chem.* **1973**, *12*, 265.

(55) Schubert, U. In *Transition Metal Carbene Complexes*; Seyferth, D., Ed.; Verlag Chemie: Deerfield Beach, FL, 1983; p 69.

(56) Hafner, A.; Hegedus, L. S.; deWeck, G.; Hawkins, B.; Dötz, K. H. *J. Am. Chem. Soc.* **1988**, *110*, 8413.

a simple consequence of the high symmetry (O_h) of this compound. The relative values for the oscillator strength are rather sensitive to a proper description of the metal-ligand and the interligand interaction. Comparing the various compounds $(CO)_5CrR$ (R = CS, PF_3, CHOH), we note that only in the case of R = CS do the low-lying excitations gain some character of the new (R) ligand.

Summary and Conclusions

Gas-phase spectra of metal carbonyls have been measured and assigned. The calculations in this study strongly suggest that the lower lying excitations in these complexes are dominated by metal-to-ligand charge-transfer excitations. In contrast to other calculations discussed in the text, we find no significant 3d-4p contribution to the observed oscillator strength below 6.2 eV (above 200 nm) in any of these complexes. Although 3d-4s excitations are calculated below 6.2 eV, only in the $Fe(CO)_5$ case is there predicted oscillator strength. Insofar as these excitations are local, they are forbidden (g-g). In the case of $Fe(CO)_5$ the band calculated at 292 nm has significant mixing with the allowed 10e' → 11e' metal-to-ligand excitation. Metal d-d excitations are not possible for $Ni(CO)_4$ but are predicted quite low-lying in $Fe(CO)_5$ and $Cr(CO)_6$, comparing well with available experimental data. Although the local nature of these d orbitals again leads to a prediction of no oscillator strength, the d-d band calculated at 430 nm in $Fe(CO)_5$ is (x,y)-allowed ($^1E'$) and should be observable as it is well separated from the next allowed band calculated at 361 nm ($^1A_2''$). The two calculated d-d excitations in $Cr(CO)_6$ at 340 and 300 are formally forbidden, but they are about 1 eV lower in energy than the first allowed band ($^1T_{1u}$ at 269 nm) and have therefore been accessible to UV spectroscopy.

As the INDO model used here has not been parametrized originally for zerovalent metal complexes such as these studied here, more detailed observations of these d-d excitations as well as of ligand-to-metal charge-transfer bands in substituted compounds would greatly help in refining the INDO/S model.

Acknowledgment. This work was supported in part by the Deutsche Forschungsgemeinschaft, the Fonds der Chemischen Industrie, and the Bund der Freunde der TU München. M.C.Z. thanks the members of the Lehrstuhl für Theoretische Chemie for their wonderful hospitality during his visit. We gratefully acknowledge the help and stimulation of Dr. Chris Culberson (Quantum Theory Project, University of Florida), Dipl.-Chem. Peter Knappe (Technische Universität München), and H.-H. Schneider.

Gas-Phase Chemistry of CH_3SOH, $^-CH_2{}^+SHOH$, $CH_3SO^\cdot$, and $^\cdot CH_2SOH$ by Neutralization-Reionization Mass Spectrometry

Frantisek Turecek,* Donald E. Drinkwater, and Fred W. McLafferty*

Contribution from the Chemistry Department, Cornell University, Ithaca, New York 14853-1301.
Received April 10, 1989

Abstract: The kinetically unstable molecules methanesulfenic acid (CH_3SOH, **1**) and its ylide isomer ($^-CH_2{}^+SHOH$, **2**) and the isomeric radicals $CH_3SO^\cdot$ and $^\cdot CH_2SOH$ exist as distinct species in the gas phase. CH_3SOH was generated by flash-vacuum pyrolysis of methyl *tert*-butyl sulfoxide and by neutralization of the corresponding cation radical. The ylide $^-CH_2{}^+SHOH$ was prepared by neutralizaton of the distonic ion, $^\cdot CH_2{}^+SHOH$, generated from di-*n*-butyl sulfoxide by double hydrogen rearrangement. Upon collisional activation CH_3SOH decomposes to $CH_3^\cdot$ and $^\cdot SOH$, while $^-CH_2{}^+SHOH$ affords mainly $^\cdot CH_2SH$ and $^\cdot OH$. Collisionally activated dissociation (CAD) spectra of the corresponding ions also distinguish these $(C,H_4,O,S)^{\cdot+}$ isomers. The isomeric radicals $CH_3SO^\cdot$ and $^\cdot CH_2SOH$ and ions CH_3SO^+ and CH_2SOH^+ were characterized through their neutralization-reionization and CAD mass spectra, respectively. Decomposition mechanisms consistent with deuterium labeling are proposed, and the relative stabilities of the (C,H_4,O,S) isomers are estimated by MNDO calculations.

Sulfenic acids,[1] R-S-OH, represent key reactive intermediates in the biologically important oxidation of thiols[2a,b] and thiolates[2c] to disulfides and sulfur oxyacids. In organic chemistry, sulfenic acids appear as intermediates in double-bond introduction by thermal decomposition of sulfoxides,[3] and synthesis of β-alkylsulfoxyenones.[4] The simplest of these, methanesulfenic acid (CH_3SOH, **1**), presumably plays a role in the photochemical oxidative degradation of methanethiol and dimethyl disulfide,[5] major natural and man-made pollutants.[5d] Investigation and analysis of **1** and other simple sulfenic acids in the condensed phase is hampered by their high propensity to undergo self-condensation to thiosulfinates.[6] Acid **1** has been generated in the gas phase by thermolysis of methyl *tert*-butyl sulfoxide (eq 1) and its structure determined from microwave spectra.[6b,c]

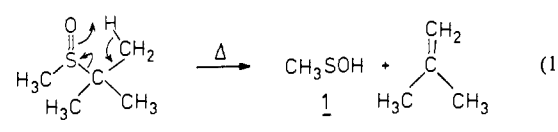

(1)

(1) Hogg, D. R. In *Comprehensive Organic Chemistry*; Barton, D. H. R., Ollis, W. D., Eds.; Pergamon: Oxford, 1979; Vol. 3, Part 11, pp 261-310. For more recent work and leading references see: Davis, F. A.; Jenkins, R. H., Jr.; Rizvi, S. Q. A.; Yocklovich, S. G. *J. Org. Chem.* **1981**, *46*, 3467-3474. Davis, F. A.; Awad, S. B.; Jenkins, R. H., Jr.; Billmers, R. L.; Jenkins, L. A. *J. Org. Chem.* **1983**, *48*, 3071-3074. Davis, F. A.; Billmers, R. L. *J. Org. Chem.* **1985**, *50*, 2593-2595. Davis, F. A.; Jenkins, L. A.; Billmers, R. L. *J. Org. Chem.* **1986**, *51*, 1033-1040.

(2) (a) Capozzi, F.; Modena, G. In *The Chemistry of the Thiol Group, Part 2*; Patai, S., Ed.; Wiley: New York,, 1974; p 785. (b) Allison, W. S. *Acc. Chem. Res.* **1976**, *9*, 293-299. (c) Hogg, D. R.; Rashid, M. A. M. *J. Chem. Res. (S)* **1988**, 160-161.

(3) (a) Trost, B. M.; Salzmann, T. N.; Hiroi, K. *J. Am. Chem. Soc.* **1976**, *98*, 4887-4902. (b) Brown, R. F. C.; Coulston, K. J.; Eastwood, F. W.; Fallon, G. D. *Aust. J. Chem.* **1986**, *39*, 189-193.

(4) (a) Davis, F. A.; Yocklovich, S. G.; Baker, G. S. *Tetrahedron Lett.* **1978**, 97-100. (b) Jones, D. N.; Cottam, P. D.; Davies, J. *Tetrahedron Lett.* **1979**, 4977-4980. (c) Bell, R.; Cottam, P. D.; Davies, J.; Jones, D. N. *J. Chem. Soc., Perkin Trans. 1* **1981**, 2106-2115.

(5) (a) Hatakeyama, S.; Akimoto, H. *J. Phys. Chem.* **1983**, *87*, 2387-2395. (b) Balla, R. J.; Heicklen, J. *J. Photochem.* **1985**, *29*, 297-310. (c) Singleton, D. L.; Irwin, R. S.; Cvetanovic, R. J. *Can. J. Chem.* **1983**, *61*, 968-974. (d) For a review see: Graedel, T. E. *Rev. Geophys. Space Phys.* **1977**, *15*, 421-428.

(6) (a) Kice, J. L.; Cleveland, J. P. *J. Am. Chem. Soc.* **1973**, *95*, 104-109. (b) Block, E., O'Connor, J. *J. Am. Chem. Soc.* **1974**, *96*, 3929-3944. (c) Penn, R. E.; Block, E.; Revelle, L. K. *J. Am. Chem. Soc.* **1978**, *100*, 3622-3623.

0002-7863/89/1511-7696$01.50/0